Superconductors

DOI: 10.1002/ange.200602614

Single-Step Synthesis and Surface-Assisted Growth of Superconducting TaS_2 Nanowires**

*Charles W. Dunnill, Hannah K. Edwards, Paul D. Brown, and Duncan H. Gregory**

The first nanostructures of layered chalcogenides observed were the scroll-like structures of WS_2 reported in 1979 as part of an investigation of dichalcogenide catalytic activity.[1] WS_2 nanotubes were subsequently characterized in 1992, generating considerable interest.[2] The nanostructured dichalcogenides of transition metals from Groups 5 and 6 have potential applications in solid-state lubricants,[3] nano-electronics,[4] hydrogen storage,[5] catalysis,[6] and as tips for scanning tunneling microscopes (STMs).[7] Tantalum disulfide (TaS_2), which has been known as a bulk compound for many decades,[8] exists in three principal polytype structures: trigonal 1T-TaS_2 ($P\bar{3}m1$), hexagonal 2H-TaS_2 ($P6_3/mmc$), and rhombohedral 3R-TaS_2 ($R3m$).[9] The 1T polytype is metastable below 550 K, but can be isolated by quenching a TaS_2 sample from above 1100 K.[10,11] In contrast, 2H-TaS_2 can be produced from 1T-TaS_2 by annealing at 823 K and is stable at room temperature.[12] The slow cooling of mixtures of the elements from high temperatures tends to yield 3R-TaS_2. The layered structures of the TaS_2 polytypes enable extensive intercalation chemistry, which combined with the inherent superconductivity of both the parent compound and its intercalated derivatives, has fuelled considerable research.[13,14] The prospect of reproducing these phenomena at the nanoscale is a tantalizing one.

Reports of TaS_2 nanostructures describe their formation by the reduction of bulk TaS_3 in an H_2 atmosphere[15] or by the pyrolysis of TaS_3 nanobelts under vacuum.[16] Both of these methods are two-step syntheses involving a trisulfide precursor. In the former report, the sensitivity of the nanomaterials to the electron beam prevented a determination of the crystal structure of the nanotubes and nanowires, whereas in the latter report, the TaS_2 nanobelts were found to adopt the rarely observed 6R polytype structure ($R\bar{3}m$). Superconductivity was observed in the 6R-TaS_2 nanobelts below 2.7 K. Herein, we report the synthesis of single-crystalline nanowires of TaS_2 by a facile one-step process, the direct heating of the elemental powders, for the first time. Our investigations aid the understanding of the polytypic nature of TaS_2 and the growth process of the material. They also indicate that the TaS_2 nanowires have enhanced superconducting properties compared to those of the bulk phase.

TaS_2 nanowires were synthesized from the elemental powders by chemical vapor transport (CVT) at elevated temperatures, in one step (see Experimental Section). Upon quenching the reaction mixture, a low-density fibrous material (LDFM) was observed on the inner surface of the reaction tube, which became free as the tube was manipulated. A black residual powder was observed at one end of the tube (**I**), and the LDFM at the opposite end (**II**; Figure 1a).

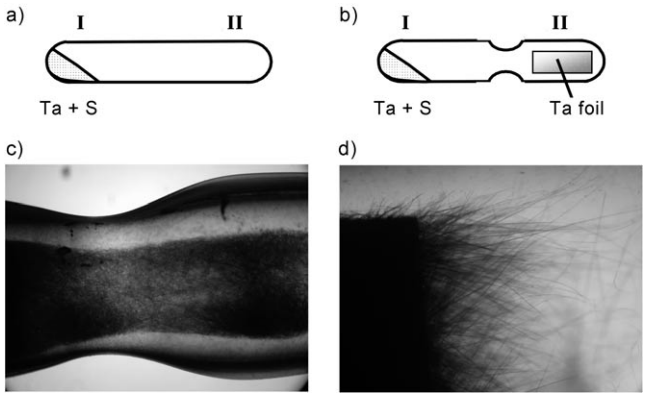

Figure 1. a) Normal and b) modified fused-silica tubes used in the synthesis of the TaS_2 nanowires. Optical microscope images showing the growth of LDFM c) within the neck of the modified tube and d) on the Ta foil.

The LDFM was easily removed after opening the ampoule, and the residual powder from region **I** was also retained. In a second series of experiments in which a Ta foil was inserted into a modified ampoule at region **II** (Figure 1b), a similar yield of LDFM was observed on the tube walls (Figure 1c), and another substantial mass of LDFM was observed on and around the Ta foil (Figure 1d). This observation suggests that the yield of nanowires may be increased through the addition of a Ta foil to the reaction ampoule. The LDFM consists of long needlelike structures growing perpendicular to the surfaces of the foil (Figure 1d).

In a control reaction with region **II** of a modified ampoule empty, we observed no nanostructure formation in this region. There was also a low yield of LDFM in, on, and around the residual powder in region **I**. A control reaction with an Fe foil in region **II** showed limited formation of LDFM in region **I** and no growth in region **II** on the Fe surface. There was, however, evidence of surface reaction on

[*] C. W. Dunnill, Prof. D. H. Gregory
Department of Chemistry
University of Glasgow
Joseph Black Building, Glasgow G12 8QQ (UK)
Fax: (+44) 141-330-4888
E-mail: d.gregory@chem.gla.ac.uk
Homepage: http://www.chem.gla.ac.uk/staff/duncang/
H. K. Edwards, Dr. P. D. Brown
School of Mechanical, Materials and Manufacturing Engineering
University of Nottingham
Nottingham NG7 2RD (UK)

[**] D.H.G. thanks the EPSRC for a DTA studentship for C.W.D. D.H.G and P.D.B thank the IDTC in Nanotechnology, University of Nottingham for a studentship for H.K.E. The authors would like to acknowledge use of the EPSRC's Chemical Database Service (ICSD) at the Daresbury Laboratory, Dr. G. S. Walker for discussions and support of H.K.E.'s work, and Mrs. N. Weston for assistance with the SEM.

Supporting information for this article is available on the WWW under http://www.angewandte.org or from the author.

the Fe foil. The brittle, lustrous layer on the surface of the Fe foil was easily removed, and analysis by powder X-ray diffraction (PXRD) and scanning electron microscopy (SEM)/energy dispersive X-ray analysis (EDX) revealed the material to be crystalline platelets of FeS (ICDD PDF 00-051-0001; Fe/S 1:1.0(1) by EDX).

PXRD patterns for the black residual powder from both series of reactions were indexed to 3R-TaS_2 (ICDD PDF 04-001-0069; $a = 3.314(4)$, $c = 17.83(2)$ Å, $R3m$). Broad peaks in the PXRD patterns for the LDFM were matched to 2H-TaS_2 (ICDD PDF 04-003-2108) as the majority phase (see Supporting Information). SEM analysis of the LDFM showed bundles of filaments with aspect ratios up to 10000:1, and no evidence of crystallites. A low-magnification view of the bundles is shown in Figure 2a. A higher-magnification image (Figure 2b) reveals that the larger microwires are clustered

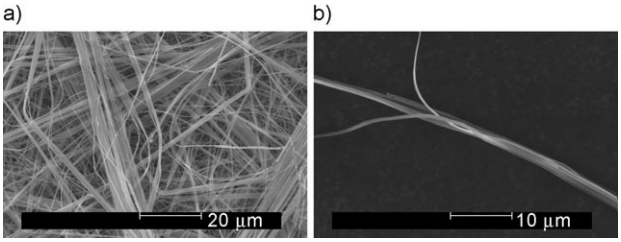

Figure 2. SEM images of TaS_2 nanowires showing a) the LDFM and b) a bundle of nanowires.

bundles of smaller individual nanofilaments. The diameters of the filaments are 100–600 nm, and their morphology is consistent for all reactions. Larger platelets of 3R-TaS_2 (identified by PXRD) were found in the residual powder in region **I**. EDX analysis of the bundles of fibers yielded a 1:1.8(3) Ta/S ratio (averaged over >20 samples). This result is in reasonable agreement to the expected 1:2 ratio, given the porous nature of the sample (for EDX, uniform polished surfaces are optimal).

Transmission electron microscopy (TEM) showed nanowire bundles of up to 1 mm in length and up to 2.5 µm in diameter. The bundles consist of very straight individual nanowires with constant diameters along their length and aspect ratios of up to 50000:1 (1 mm:20 nm; Figure 3a). The nanowires displayed selected area electron diffraction (SAED) patterns consistent with a single-crystalline material (Figure 3a, inset).

The multifilamentary morphology of the nanowires suggests a cooperative growth mechanism, whereby a number of nanowires nucleate and simultaneously propagate along one crystallographic direction. This morphology is further illustrated by the large bundle shown in Figure 3b: the numerous crystalline TaS_2 filaments in the bundle lead to a varied contrast across the wire. The nanowire bundle appears to have fractured during sample preparation, hence, taking on an uneven terminal edge. The corresponding SAED pattern, shown in [0001] projection in Figure 3c, is characteristic of those produced by the nanowires, consisting of sharp spots in a hexagonal array.

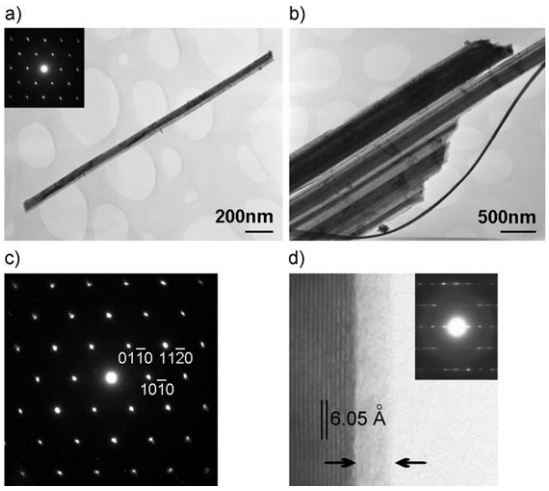

Figure 3. a) Bright-field TEM image of a single-crystalline TaS_2 nanowire and the corresponding SAED pattern in [0001] projection (inset). b) Bright-field TEM image of a bundle of nanowires and c) the corresponding SAED pattern in [0001] projection (indexed to the 2H-TaS_2 cell). d) Phase-contrast TEM image of a nanowire, showing lattice fringes with a spacing of 6.05 Å and an amorphous oxide layer (arrows), and the corresponding SAED pattern in approximately $[2\bar{1}\bar{1}0]$ projection (inset).

As the crystal structures of the 2H- and 1T-TaS_2 polytypes differ in the stacking of layers along the [0001] direction, leading to differences in the c parameters, the [0001] projections of the SAED patterns of the two polytypes are similar; hence, the diffraction pattern in Figure 3c could be indexed to either structure. However, careful analysis of this and further SAED patterns, such as that shown in the inset to Figure 3d, which approaches a $[2\bar{1}\bar{1}0]$ projection, yields a more precise match to 2H-TaS_2 than to 1T-TaS_2. The 3R and less-common 6R polytypes[9,17] were also considered, but neither provided an acceptable match to the SAED data. Therefore, the SAED data are consistent with the predominant phase of the nanowires being 2H-TaS_2.[9] This assignment concurs with previous work, where nanostructures produced through the reduction of TaS_3 with H_2 were tentatively identified as 2H-TaS_2, on the basis of PXRD data.[18] However, TaS_2 nanobelts prepared from the heating of TaS_3 under vacuum were reported to adopt the 6R structure.[16] Analysis of SAED patterns for the nanowires found that the $11\bar{2}0$ diffraction spots were coincident with the long axis of the nanowires, indicating that growth occurs along the $\langle 11\bar{2}0\rangle$ directions.

Upon rotating the nanowires around their longitudinal axes, lattice fringes were observed parallel to the nanowire surface (Figure 3d). The fringe spacing is 6.05(8) Å, in good agreement with the (0002) plane spacing of 2H-TaS_2 (6.0485 Å), but in poor agreement with the equivalent (0001) spacing of the 1T polytype (5.8971 Å), again suggesting that the 2H-TaS_2 is the dominant phase of the nanowires. The measurement was calibrated for magnification and image resolution using the known $(10\bar{1}0)$ fringe spacing of Nb_3Te_4. The corresponding SAED pattern, which approaches a $[2\bar{1}\bar{1}0]$ projection, highlights the diffraction spacings corresponding to the (0002) planes (Figure 3d, inset). An amorphous film

was also observed on the surface of the wires, which most likely originates from surface oxidation upon exposure to air, as has been observed in other systems.[19]

The nanowires exhibit superconductivity, with an onset temperature of 3.4 K (Figure 4). This behavior is in stark

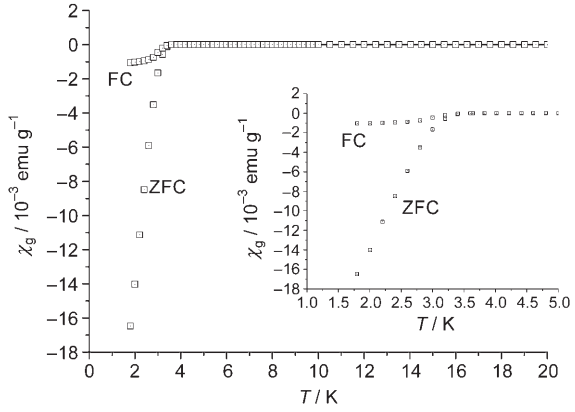

Figure 4. Temperature dependence of the magnetic susceptibility (χ_g) of the TaS_2 nanowires, under FC and ZFC conditions. The temperature region near the superconducting transition at $T_c = 3.4$ K is highlighted (inset).

contrast with that of bulk 2H-TaS_2, which exhibits superconductivity below 1 K ($T_c = 0.6$[14] or 0.8 K[20]). Further, the transition temperature of the 2H-TaS_2 nanowires is higher than that reported for the 6R-TaS_2 nanobelts ($T_c = 2.7$ K).[16] Bulk 6R-TaS_2 has been reported to exhibit superconductivity, with $T_c = 2.3$ K at ambient pressure and $T_c > 4$ K at 17.3 kbar.[21] As discussed with respect to 6R-TaS_2 nanobelts[16] based on the arguments of by Friend and Yoffe,[22] the increased transition temperatures of the nanomaterials, relative to that of the bulk material, could originate from a suppression of the periodic lattice distortion that drives charge density wave formation. A similar mechanism leads to an enhancement of the transition temperature of bulk 2H-TaS_2 following intercalation ($T_c = 2$–5.5 K) or the application of pressure. This effect may also be responsible for the observation of elevated transition temperatures in nanowires and nanotubes of $NbSe_2$,[23] for which electronic-structure calculations have predicted a high density of states (DOS) at the Fermi level (dominated by Nb 4d states).[24] Importantly, similar calculations have predicted broadly analogous effects for nanostructured 2H-TaS_2 and the likelihood of superconductivity.[25] Furthermore, when nanowires are arranged in bundles a "conductivity strengthening effect" occurs;[26] for example, semiconducting $B_xC_yN_z$ nanotubes become metallic,[27] and metallic single-walled C nanotubes become superconducting.[28] Thus, an increase in the superconducting transition temperature might occur when TaS_2 nanowires form bundles. This effect might also contribute to the increase in transition temperature from TaS_2 nanobelts to nanowire bundles.

In summary, we have exploited a simple one-step synthesis to produce superconducting TaS_2 nanowire bundles. These high-aspect-ratio wires, which adopt the 2H structure, exhibit superconductivity below $T_c = 3.4$ K. The nanowire bundles can be produced by using a surface-assisted growth process, which could find application in the selective synthesis of other dichalcogenide materials with enhanced electronic properties.

Experimental Section

In a typical reaction, elemental powders of Ta (99.9%, −325 mesh, Aldridge) and S (99.5%, Fisher) were ground together in a 1:2 Ta/S ratio and sealed in a 12-mm-diameter fused-silica tube under a vacuum of 4×10^{-5} Torr. The tube was placed horizontally in a box furnace and heated to 650–1000 °C for up to 70 h. It was then air quenched to room temperature and opened. The products were easily separated using tweezers.

In alternative reactions, 1:2 mixtures of the elemental powders were placed at one end (**I**) of a fused-silica tube with a width restriction (neck) halfway along its length (Figure 1a). A piece of Ta foil ($10 \times 30 \times 0.25$ mm^3, 99.9%, Aldridge) was placed at the opposite end (**II**) of the tube. The reactants were, thus, prevented from coming into direct physical contact with the foil as the tube was sealed or during the reaction. The tube was heated to 650 °C for up to 70 h, and the products were separated by mechanical methods. Two different control experiments were also run, in which region **II** either remained empty or contained Fe foil ($10 \times 30 \times 0.25$ mm^3, 99.9%, Aldridge). Fe is known to have catalytic effects on the formation of nanowires,[29–31] and was therefore a clear choice for comparison.

The products of the reactions were characterized by PXRD (Philips X'Pert diffractometer; θ–2θ; $Cu_{K\alpha}$ radiation), SEM (Philips XL30 SEM and XL30 ESEM-FEG, both with Oxford Instruments ISIS EDX systems; samples prepared by depositing powder on a C tab), TEM (JEOL 2000fx TEM and ISIS EDX system; samples prepared by sonicating powder in acetone and then pipetting drops of the suspension onto holey-C-film Cu grids), and magnetometry (Quantum Design MPMS 5T; field-cooled (FC) and zero-field-cooled (ZFC) measurements with an applied field of 10 Oe over 1.8–20 K; samples loaded into gelatin capsules).

Received: June 30, 2006
Published online: September 28, 2006

Keywords: chalcogenides · nanostructures · sulfur · superconductors · tantalum

[1] R. R. Chianelli, E. Prestridge, T. Pecorano, J. P. DeNeufville, *Science* **1979**, *203*, 1105.
[2] R. Tenne, L. Margulis, M. Genut, G. Hodes, *Nature* **1992**, *360*, 444.
[3] S. Prasad, J. Zabinski, *Nature* **1997**, *387*, 761.
[4] O. Tal, M. Remskar, R. Tenne, G. Haase, *Chem. Phys. Lett.* **2001**, *344*, 434.
[5] J. Chen, N. Kuriyama, H. Yuan, Hiroyuki T. Takeshita, T. Sakai, *J. Am. Chem. Soc.* **2001**, *123*, 11813.
[6] J. Chen, S.-L. Li, Q. Xu, K. Tanaka, *Chem. Commun.* **2002**, 1722.
[7] R. Tenne, *Chem. Eur. J.* **2002**, *8*, 5296.
[8] H. Biltz, C. Kircher, *Ber. Dtsch. Chem. Ges.* **1910**, *43*, 1636.
[9] F. Jellinek, *J. Less-Common Met.* **1962**, *4*, 9.
[10] J. A. Wilson, F. J. DiSalvo, S. Mahajan, *Adv. Phys.* **2001**, *50*, 1171.
[11] J. F. J. Revelli, W. A. Phillips, *J. Solid State Chem.* **1974**, *9*, 176.
[12] J. F. Revelli, *Inorg. Synth.* **1979**, *19*, 35.
[13] S. F. Meyer, R. E. Howard, G. R. Stewart, J. V. Acrivos, T. H. Gaballe, *J. Chem. Phys.* **1975**, *62*, 4411.

[14] A. Schlicht, M. Schwenker, W. Biberacher, A. Lerf, *J. Phys. Chem. B* **2001**, *105*, 4867.
[15] M. Nath, C. N. R. Rao, *J. Am. Chem. Soc.* **2001**, *123*, 4841.
[16] X. Wu, Y. Tao, Y. Hu, Y. Song, Z. Hu, J. Zhu, L. Dong, *Nanotechnology* **2006**, *17*, 201.
[17] G. Hagg, N. Schonberg, *Ark. Kemi* **1954**, *7*, 371.
[18] M. Nath, C. N. R. Rao, *Pure Appl. Chem.* **2002**, *74*, 1545.
[19] a) Y. Z. Jin, W. K. Hsu, Y. L. Chueh, L. J. Chou, Y. Q. Zhu, K. Brigatti, H. R. Kroto, D. R. M. Walton, *Angew. Chem.* **2004**, *116*, 5788; *Angew. Chem. Int. Ed.* **2004**, *43*, 5670; b) H. K. Edwards, P. A. Salyer, M. J. Roe, G. S. Walker, P. D. Brown, D. H. Gregory, *Angew. Chem.* **2005**, *117*, 3621; *Angew. Chem. Int. Ed.* **2005**, *44*, 3555.
[20] F. J. DiSalvo, R. Schwall, T. H. Geballe, F. R. Gamble, J. H. Osiecki, *Phys. Rev. Lett.* **1971**, *27*, 310.
[21] E. Figueroa, Y.-K. Kuo, A. Olinger, M. A. Lloyd, L. D. Bastin, S. Petrotsatos, Q. Chen, B. Dobbs, S. Dev, J. P. Selegue, L. E. DeLong, C. P. Brock, J. W. Brill, *J. Solid State Chem.* **1995**, *114*, 486.
[22] R. H. Friend, A. D. Yoffe, *Adv. Phys.* **1987**, *36*, 1.
[23] a) M. Nath, S. Kar, A. K. Raychaudhuri, C. N. R. Rao, *Chem. Phys. Lett.* **2003**, *368*, 690; b) Y. S. Hor, U. Welp, Y. Ito, Z. L. Xiao, U. Patel, J. F. Mitchell, W. K. Kwok, G. W. Crabtree, *Appl. Phys. Lett.* **2005**, *87*, 142506.
[24] V. V. Ivanovskaya, A. N. Enyashin, N. I. Medvedeva, A. L. Ivanovskii, *Phys. Status Solidi B* **2003**, *238*, R1.
[25] A. N. Enyashin, I. R. Shein, N. I. Medvedeva, A. L. Ivanonskii, *Internet Electron. J. Mol. Des.* **2005**, *4*, 316, http://www.biochem-press.com.
[26] V. V. Pokropivnyi, *Powder Metall. Met. Ceram.* **2002**, *41*, 123.
[27] X. Blase, J.-C. Charlier, A. De Vita, R. Car, *Appl. Phys. Lett.* **1997**, *70*, 197.
[28] M. Kociak, A. Y. Kasumov, S. Gueron, *Phys. Rev. Lett.* **2001**, *86*, 2416.
[29] J.-Y. Raty, F. Gygi, G. Galli, *Phys. Rev. Lett.* **2005**, *95*, 096103.
[30] Y. Homma, Y. Kobayashi, T. Ogino, *J. Phys. Chem. B* **2003**, *107*, 12161.
[31] Z. P. Huang, D. Z. Wang, J. G. Wen, M. Sennett, H. Gibson, Z. F. Ren, *Appl. Phys. A* **2002**, *74*, 387.

